Optical properties in the infrared range of the birefringent α-GeO2 single crystal

Pascale Armand, Patrick Hermet, Jean-Louis Bantignies, Abel Haidoux, David Maurin, Bertrand Ménart, Alexandra Peña, Philippe Papet

Optical properties in the infrared range of the birefringent α-GeO_2 single crystal

Pascale Armand[a*], Patrick Hermet[a], Jean-Louis Bantignies[b], Abel Haidoux[a], David Maurin[b], Bertrand Ménart[c], Alexandra Peña[c], and Philippe Papet[a]

[a] ICGM, Université de Montpellier, CNRS, Montpellier, France

[b] L_2C, Université de Montpellier, CNRS, Montpellier, France

[c] Institut Néel, CNES, Dpt Matière Condensée, Matériaux et Fonctions, 25, Avenue des Martyrs, bât. F, BP 166, 38042 Grenoble Cedex 09, France

Corresponding author

*E-mail : pascale.armand@umontpellier.fr; Tel : +33 (0)4 67 14 33 19

ORCID : 0000-0001-8921-5427.

Abstract

The components of the frequency-dependent complex refractive index were determined indirectly for the new non-centrosymmetric α-GeO_2 crystal using polarized Fourier transform infrared reflectivity spectra measured in the far- and mid-infrared spectral region at room temperature. All the longitudinal- and transverse-optical infrared active modes with E and A_2 symmetry, according to the D_3 point group, were identified and localized within the 100-1000 cm^{-1} range in very good agreement with a previous first-principles based calculation. For the A_2- and E-type modes, both the longitudinal- and transverse-optical splitting were detected. The refractive indices n_o ($\vec{E} \perp c$) and n_e ($\vec{E} // c$) in the infrared domain present considerably higher values than the ones observed in the visible light range, and the high birefringence would find application in many optical devices.

KEYWORDS: A. oxides, B. optical properties, C. infrared spectroscopy

1. Introduction

Optical devices operating in the far- and mid-infrared (FIR and MIR) domains are sought after for applications and oxides have a lot of interest because of their chemical and thermal stability. Regarding the new non-centrosymmetric α-GeO_2 single-crystal, no information about its optical properties in the infrared domain is available to our knowledge. The colorless, transparent and non-toxic α-GeO_2 material crystallizes with an α-quartz structure and high-quality single-crystals have recently been grown using the flux method [1,2]. This uniaxial allotropic form of GeO_2 was recently investigated as a promising piezoelectric material for very-high temperature applications [2-4]. This phase, with a large band gap, has been shown to be chemically, structurally and mechanically stable up to its melting at 1116°C and its piezoelectric properties are maintained up to the higher investigated temperature, 1000°C [3,5,6]. The reported properties of the α-GeO_2 material suit already several requirements in the guideline to help in the selection of the right material for a given application in the infrared domain.

α-GeO_2 presents a trigonal structure (*P*$3_1$21 or *P*$3_2$21 space group) and contains three formula units per unit cell (Z=3) [1]. The zone-center optical phonons can be sorted according to the irreducible representations of the D_3 point group as $8E \oplus 4A_2 \oplus 4A_1$, where the E-representation is both infrared and Raman active and the A_2 (resp. A_1) representation is infrared (resp. Raman) active [7]. Due to the absence of an inversion center in the α-GeO_2 structure, the macroscopic electric field splits the polar modes (infrared modes) in transverse-optical (TO) and longitudinal-optical (LO) modes close to the center of the Brillouin zone. Several experimental studies have been carried out to assign the zone-center phonon modes of α-GeO_2. However, the Raman intensity of at least two E (TO) modes between 200 and 350 cm^{-1} is extremely small to be unambiguously assigned and some discrepancies can be

observed between the different sets of infrared data reported in the literature, especially within the 200-400 cm^{-1} range [8-12]. These differences could be the consequence of the difficulty of obtaining large-size, high-quality α-GeO_2 single-crystals and of the lack of polarized data. Until now, the infrared A_2 (LO) phonon modes of α-GeO_2 have never been measured, leaving the strength of their LO-TO splitting unknown.

The present paper deals with the investigation of the optical properties of the germanate, α-GeO_2. We present the first report on the polarized infrared reflectivity of the anisotropic trigonal form of GeO_2. It was registered on a high-quality plate prepared from a water-free flux-grown single-crystal. Using the classical dispersion theory, the oscillator strength and the damping of the polar modes have been derived from the reflectivity spectra. Depending on the orientation of the electric field in relation to the *c* optical axis (perpendicular or collinear), the frequency-dependent complex dielectric functions in the infrared region are reported with the refractive indices. The birefringence Δn is calculated from the n_e-n_o difference.

2 Experimental section

The trigonal, non-centrosymmetric form of the germanium oxide α-GeO_2 was obtained as colorless, high-transparent, and large-size single-crystals using the top-seeded solution growth technique. Details on the experimental crystal growth conditions were already published [2]. The as-grown GeO_2 single-crystals are characterized by high-quality and an absence of OH group identification via spectroscopy techniques [1,2,4].

Using a Cartesian coordinate system, α-GeO_2 plates cut perpendicular to $[2\bar{1}0]$, $[010]$ and $[001]$ directions are known as X-, Y-, and Z- cuts respectively, with the center of the plate at the origin. The Z-axis of the coordinate system coincides with the natural *c*-axis of the crystal. Infrared spectra were collected using a mechanically polished face of a Y-cut plate

(containing the *c*-optical axis) of an α-GeO_2 single crystal as presented in Fig. 1. The thickness was 250 μm.

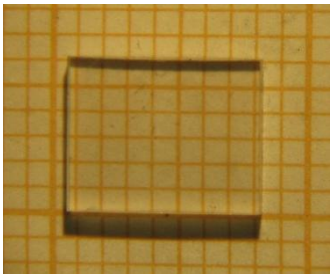

Fig. 1 α-GeO_2 Y-cut plate.

Reflection spectra have been recorded using a Bruker IFS 66V Fourier transform spectrometer covering the 40 – 8000 cm^{-1} spectral range following the configuration described in Fig. 2. In the FIR domain, a 6μ-Mylar beam splitter, a mercury discharge lamp, and a Si-bolometer detector cooled at 4.6 K were used. In the MIR domain, a black body source, a KBr beam splitter, and a deuterated triglycine sulfate (DTGS) detector were used. Room-temperature polarized reflectance measurements were performed with the reflection Bruker accessory (A510 Q/T) with an angle of incidence (θ) of 11° placed in the sample compartment of the FTIR spectrometer. KRS5 (Thallium Bromide) Wire grid polarizer was used in the MIR and polyethylene polarizer in the FIR. The polarizer was installed upstream of the reflection accessory. The infrared reflectance signal was collected on a Y-cut with the polarization of the incident light as $\vec{E}//c$ and $\vec{E}\perp c$.

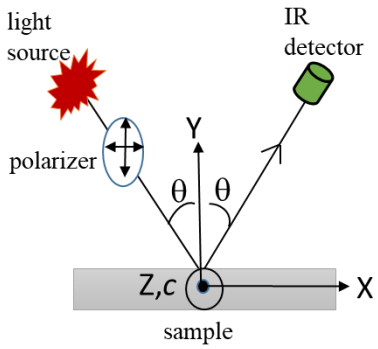

Fig. 2 Schematic representation of the beam geometry for the polarized infrared reflectance measurements.

To determine the resonant frequencies of the active infrared modes, we have adopted a simple classical dispersion model to fit the reflectance data using the RefFIT software [13].

3 Results and discussion

The experimental reflectivity data for a sample of semi-infinite thickness can be analyzed by the reflectance curve fitting using a theoretical model for the dielectric function [14].

At normal incidence, the reflectivity spectrum, R (ω), can be calculated according to the Fresnel equation:

$$R(\omega) = \left|\frac{1-\sqrt{\varepsilon(\omega)}}{1+\sqrt{\varepsilon(\omega)}}\right|^2 \qquad (1)$$

The contribution of *k* polar phonon modes to the dielectric function, ε (ω), at photon energy ħω, can be expressed using a factorized model with Lorentzian broadening:

$$\varepsilon_j(\omega) = \varepsilon_j^{\infty} \prod_{i=1}^{k} \frac{\omega_{ij,LO}^2 - \omega^2 - i\omega\gamma_{ij,LO}}{\omega_{ij,TO}^2 - \omega^2 - i\omega\gamma_{ij,TO}} \qquad (2)$$

where *j* is equal to "//" or "⊥", which denotes the dielectric functions and phonon frequencies parallel or perpendicular to the optical *c* axis. ω_{ij}(LO) and γ_{ij}(LO), (resp. ω_{ij}(TO) and γ_{ij}(TO)) are the phonon frequency and the broadening value of the i^{th} LO (resp. TO) phonon,

respectively. The $\varepsilon^{\infty}_{//}$ and $\varepsilon^{\infty}_{\perp}$ model parameters are the high-frequency dielectric constants for polarization parallel and perpendicular to the optical axis, respectively.

The experimental optical phonon assignments of the α-GeO_2 structure, previously reported in the literature, are given in Table 1. They are localized below 1000 cm^{-1}. Most of the experimental infrared absorption data sets of α-quartz-like GeO_2 were recorded on commercial powder with no information on the purity and crystalline quality [9,11,12]. The measured α-GeO_2 single-crystal was obtained at low-temperature via a refluxed hydrothermal solution and it contains high-level of OH groups [10].

Table 1 Experimental infrared absorption frequencies (in cm^{-1}) with their symmetry (when available) recorded on an α-GeO_2 sample at room temperature.

Powder [8]	**Powder [9]**	**Single crystal [10]**	**Powder [11]**	**Powder [12]**
122 (E)	124			
209 (E)	212			
249 (A_2)				
265 (E)				
332 (E)	332	336	332 (E)	
345 (A_2)			345 (A_2)	
491 (E)	518	515	515 (A_2)	
540 (A_2)	554	560	540 (E)	
585 (E)	584	583	585 (A_2)	
				723
				728
				752
				803
				846 (E, TO)
				851 (A_2, TO)
882 (A_2)	886	874	885 (A_2+E)	887 (A_1)
				937 (E, LO)
962 (E)	958	960	963 (E)	962 (A_2, LO)

Despite the relative simplicity of the hexagonal GeO_2 structure, there are many contradictions and ambiguities concerning the number of TO modes, their frequency position and their symmetry mode attribution between the different sets of experimental data, Table 1. Furthermore, information on most of the LO modes is missing. To solve these problems unambiguously, we have undertaken polarized infrared reflectivity measurements on a high-quality, water-free α-GeO_2 single-crystal grown by the high-temperature flux method. Fig. 3 displays the polarized infrared reflectivity spectra for a Y-cut orientation, measured at room-temperature. This orientation allows us to probe both the E-type modes (electric field of the infrared radiation perpendicular to the *c* optical axis) and the A_2-modes (electric field of the infrared radiation collinear to the optical axis).

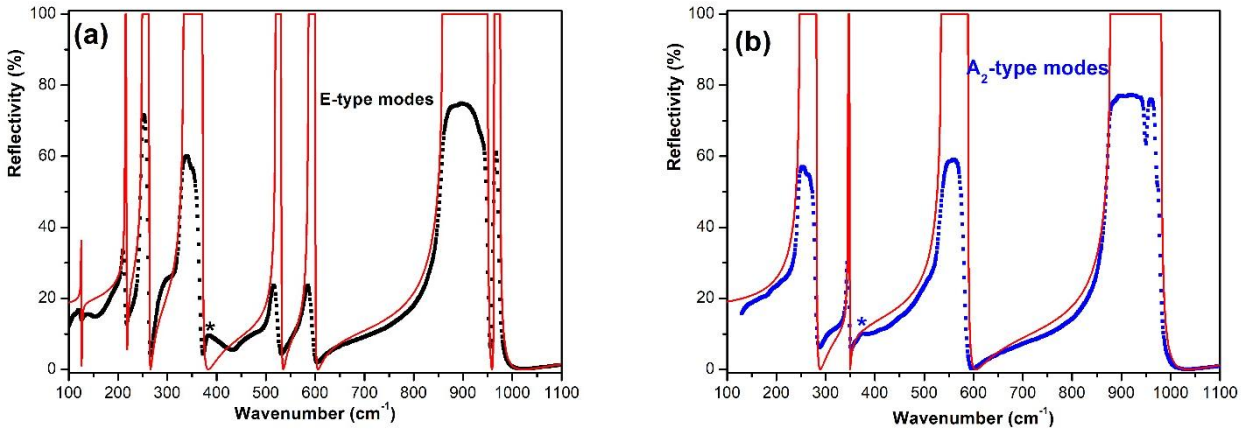

Fig. 3. Polarized infrared reflectivity spectra in α-GeO_2 (a) E-modes and (b) A_2-modes. The dash lines show room-temperature experimental data (present) and the solid lines represent the calculated spectra [7] at 0 K using the density functional theory. The asterisks correspond to nonphysical features due to artifacts originating from strong absorbance of polyethylene used in beam splitter and polarizer between 350 and 450 cm^{-1}.

With the experimental data, we report in Fig. 3 a previous density functional theory (DFT) based calculation performed by our group at the LDA level (see [7] for the computational details). The calculated reflectivity intensity saturates to the unity as the

damping of the phonon modes has been neglected in our calculations. Nevertheless, this does not call into question our modes assignment as the calculated infrared reflectivity profile is similar to the experimental data.

According to the group theory, eight experimental bands associated with E-type mode were observed around 120, 210, 250, 330, 510, 580, 860 and 980 cm^{-1} (Fig. 3a). The reflectance spectrum registered in the same conditions on a Z-cut GeO_2 plate [001] for which only the E-type modes can be observed, confirms this result. Our DFT calculation supports the E-band existence near 120 cm^{-1} despite its small experimental intensity.

Similarly, the calculated infrared reflectivity profile of the A_2 modes is in excellent agreement with the experimental one, Fig. 3b. Four experimental bands are observed, as expected by the group theory, around 250, 345, 540 and 900 cm^{-1}. The experimental features, observed at 950 and 980 cm^{-1}, can be attributed to off specular reflectivity related to the anisotropic nature of α-GeO_2 and they were not being taken into account.

The excellent agreement between our experimental spectra and the calculated ones highlights the high-quality of the as-grown α-GeO_2 single-crystals with the high-temperature flux method.

The parameters that yield the best fit of the polarized infrared measurements, including the high-frequency dielectric constants and phonon modes (ω (TO) and ω (LO)) in Eq. (2), can be obtained by minimizing the mean-square deviation. They are listed in Table 2 for both the E-type and A_2-type modes. The results are compared to 300 K polarized Raman data obtained on flux-grown α-GeO_2 single-crystal and with first-principle based calculations. The thermal dependence of phonon modes and the slight volume underestimation obtained at the LDA level can be at the origin of the small differences observed between the experimental (300K) and the calculated (0K) frequencies. Concerning the eight doubly degenerate E-modes, we have an excellent agreement between the infrared frequency of the TO/LO modes and the

ones coming from polarized Raman experiments and DFT (Table 2) [4,7]. For the first time, the A_2 (LO) frequencies are experimentally determined for non-centrosymmetric GeO_2 crystal and they are in perfect agreement with those calculated at 0 K by DFT [7]. For both E- and A_2-type modes, the splitting value is consistent with the DFT prediction. This excellent experiment-calculation agreement supports our fitting parameters and allows us to unambiguously identify and assign the whole infrared phonon modes.

Table 2. The fitting parameters along with previous experimental polarized Raman work and DFT based calculation [4,7]. The symmetry assignment of the phonons is given in the first column. The frequency (ω) and damping (γ) of modes are in cm^{-1}. The high-frequency dielectric constants (ε^{∞}) are dimensionless.

	Expt. (Infrared)				**Expt. (Raman [4])**	**Calc. (DFT [7])**
Symmetry	ω_{TO}	γ_{TO}	ω_{LO}	γ_{LO}	ω_{TO} / ω_{LO}	ω_{TO} / ω_{LO}
E	120.0	5.7	120.4	6.2	123/124	126/126
E	212.5	6.8	216.2	5.5	212/215	212/218
A_2	250.1	14.9	283.2	12.5		247/282
E	250.0	2.8	262.2	6.3	248/263	248/263
E	330.2	17.8	368.0	17.5	329/367	332/372
A_2	343.4	6.5	349.7	8.6		345/348
E	517.0	12.3	524.0	7.2	517/527	519/531
A_2	533.7	25.9	582.3	6.5		534/89
E	584.5	21.1	597.5	7.2	586/599	586/600
E	861.9	10.2	950.4	5.7	859/952	858/950
A_2	874.9	15.1	976.4	7.9		877/981
E	958.5	5.2	971.5	2.7	961/973	963/976
$\varepsilon_{\parallel}^{\infty}$	2.67					3.04
$\varepsilon_{\perp}^{\infty}$	2.56					2.95

Considering the high-frequency dielectric constants, Table 2, we observe that $\varepsilon_{\parallel}^{\infty} > \varepsilon_{\perp}^{\infty}$ and that the values are in the same range as those obtained via 0 K DFT calculations

[7]. The over-estimation of the DFT dielectric constants compared to the experimental ones is usual when using LDA exchange-correlation functional [15]. This problem is linked to the underestimation of the electronic band gap and the lack of polarization dependence of local (LDA) exchange-correlation functional. To overcome this problem, it is a common practice to apply the so-called "scissors correction", in which we use an empirical rigid shift of the conduction bands to adjust the LDA band gap to the experimental value [16]. Considering the experimental band gap E_g of 5.94 eV, we fix the scissors correction to 1.99 eV [2]. The calculation of ε^{∞} using the experimental lattice parameters and a scissors correction decreases the DFT values given in Table 3 to $\varepsilon^{\infty}_{//}$ = 2.62 and $\varepsilon^{\infty}_{\perp}$ = 2.55, which are in excellent agreement with the experimental values.

TO and LO phonon frequencies can be respectively determined from the maxima and minima of the modulus of the dielectric constant $|\varepsilon| = (\varepsilon'^2 + \varepsilon''^2)^{1/2}$ where ε' and ε'' are the real and imaginary part of the complex dielectric function. The determination of the LO mode frequencies is also possible from the peak frequencies of the dielectric loss function,

$-\mathrm{Im}(\varepsilon^{-1}) = \varepsilon'' / (\varepsilon'^2 + \varepsilon''^2)$.

Fig. 4 displays these functions and all the reststrahlen bands can be identified. These functions can be also useful for Kramers-Kronig transformations.

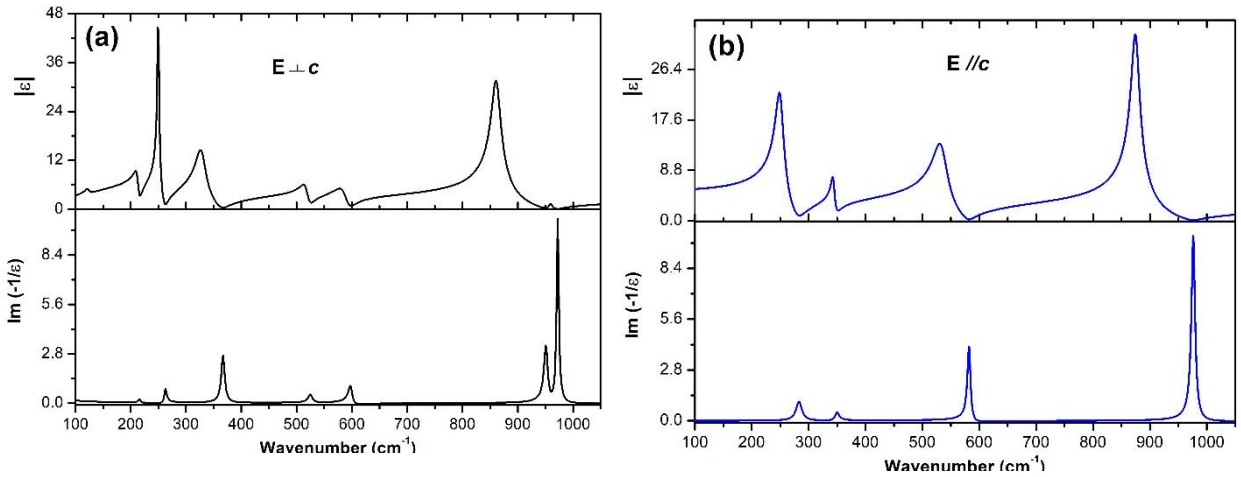

Fig. 4 Modulus of the dielectric constant and dielectric loss function of α-GeO_2 for (a) $\vec{E}\perp c$ (E-type modes) and (b) $\vec{E}//c$ (A_2-type modes).

The refractive indices $n(\omega) = [½ (\varepsilon'(\omega) + |\varepsilon(\omega)|)]^{1/2}$ calculated using parameters given in Table 2, are displayed in Fig. 5(a) in the infrared range between 100 and 1000 cm^{-1}. n_e and n_o denote the extraordinary ($\vec{E}//c$) and ordinary ($\vec{E}\perp c$) refractive indices, respectively. It should be emphasized that the refractive indices n_o and n_e of α-GeO_2 in the FIR-MIR domain are below unity in the wavelength ranges of 250-400 cm^{-1}, 550-600 cm^{-1}, and over 880 cm^{-1} and that, they present considerably higher values than visible light refractive indices [3]. The mean refractive index $n = (2n_o+n_e)/3$ is in very good agreement with the one extracted from spectroscopic ellipsometry measurements on hexagonal GeO_2 films in the 333-2000 cm^{-1} range [17]. These excellent properties would make α-GeO_2 a type of significant material for infrared optics.

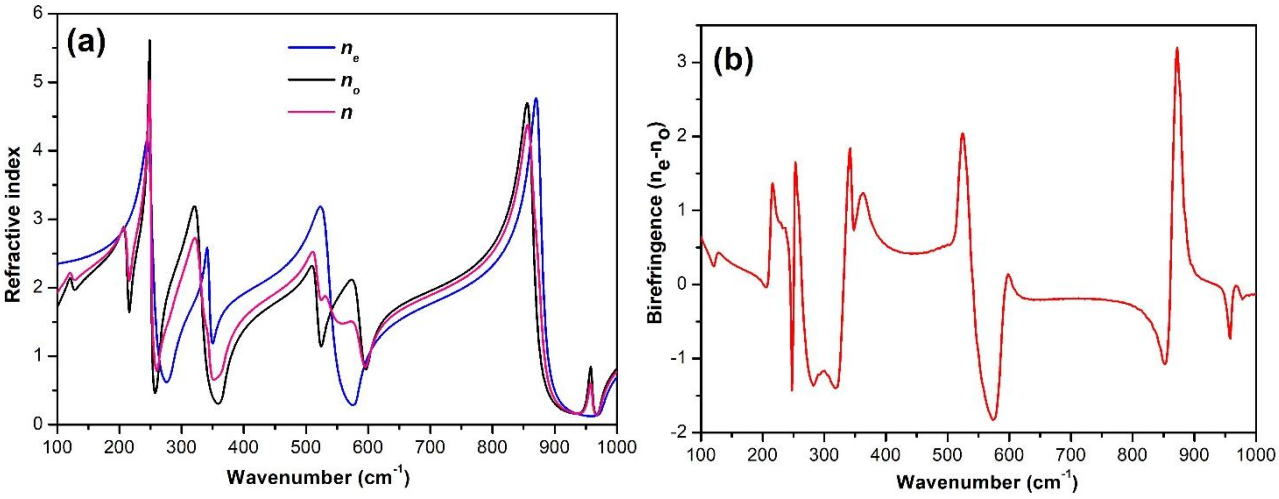

Fig. 5 (a) Extraordinary (n_e) and ordinary (n_o) refractive indices obtained from the dispersion fit to the reflectance data of Fig. 1 and (b) optical birefringence of α-GeO_2 in the FIR –MIR domain. The parameters are dimensionless.

The uniaxial α-GeO_2 material presents a large birefringence Δn in the FIR-MIR domain, Fig. 5(b), according to the difference n_e-n_o, with a value of Δn up to -3.15 at 873 cm^{-1} and 1.54 at 253 cm^{-1}. In comparison, the refractive-index difference of α-GeO_2 in the visible spectral domain is about 0.026. For example, at 514.5 nm, n_o=1.651, n_e=1.677 and Δn=0.0258 [3]. This high birefringence ability in the far- and mid-IR window would find application in many optical devices, such as wave plates, polarizing prisms, light modulators, beam displacers, and beam splitters.

4 Conclusion

We have shown that all of the TO and LO-type IR fundamentals for both the E-type and A_2-type modes of the uniaxial non-centrosymmetric α-GeO_2 material can be resolved from the polarized reflectivity spectra. Furthermore, an excellent agreement was found with the first-principles based calculation report of the FIR and MIR phonon frequencies and the splitting values. These results fix the contradictions and ambiguities concerning the number of TO modes, their frequency position and their symmetry mode attribution and they give, for the first time, experimental information on the A_2 (LO) modes.

Some physical properties of α-GeO_2 in the infrared domain that are missing in the literature, have indirectly been obtained from this polarized reflectivity study such as the frequency-dependent dielectric constants and the intrinsic optical constants, the refractive indices. The ordinary and extraordinary α-GeO_2 refractive indices present considerably higher values than the visible-light refractive indices. The same evolution is found for the birefringence deduced from n_e-n_o difference.

These room-temperature optical properties, coupled with its mechanical robustness and its toxic substance-free, would make α-GeO_2 a significant material for infrared optical devices in the sensing, imaging, and communication fields and bulk optics (lenses, prisms,

beam splitters, etc.) for example. Furthermore, as α-GeO_2 is chemically and structurally stable up to its melting temperature (1100°C) thus, this dielectric material could be associated to devices operating at very high temperature.

Acknowledgment

Infrared Reflectance experiments were performed at the IR-Raman technological platform of the University of Montpellier, France.

Funding

This work was supported by the French Research National Agency ANR [grant number 14-CE07-0017].

References

1 A. Lignie, D. Granier, P. Armand, J. Haines, P. Papet, Modulation of quartz-like GeO_2 structure by Si substitution: an X-ray diffraction study of $Ge_{1-x}Si_xO_2$ ($0 \leq x < 0.2$) flux-grown single crystals. J. Appl. Cryst. 45 (2012) 272-278.

2 A. Lignie, B. Ménaert, P. Armand, A. Peña, J. Debray, P. Papet; Top-Seeded Solution Growth and Structural Characterizations of α-quartz-like Structure GeO_2 Single Crystal, Cryst. Growth Des. 13 (2013) 4220-4225.

3 A. Lignie, W. Zhou, P. Armand, B. Ruffle, R. Mayet, J. Debray, P. Hermet, B. Ménaert, P. Thomas, P. Papet, High-temperature Elastic moduli of Flux-grown α-GeO_2 Single Crystal, ChemPhysChem 15 (2014) 118-125.

4 G. Fraysse, A. Lignie, P. Hermet, P. Armand, D. Bourgogne, J. Haines, B. Ménaert and P. Papet, Vibrational origin of the thermal stability in the highly distorted α-quartz-type material GeO_2, an experimental and theoretical study, Inorg. Chem. 52 (2013) 7271-7279.

5 A. Lignie, P. Armand, P. Papet, Growth of piezoelectric water-free GeO_2 and SiO_2-substituted GeO_2 single crystals, Inorg. Chem. 50 (2011) 9311-9317.

6 Philippe Papet, Micka Bath, Abel Haidoux, Benoit Ruffle, Bertrand Menaert, Alexandra Peña, Jérôme Debray, Pascale Armand
High-temperature piezoelectric properties of flux-grown α-GeO_2 single crystal, J. Appl. Phys. 126 (2019) 144102.

7 P. Hermet, G. Fraysse, A. Lignie, P. Armand, Ph. Papet, Density Functional Theory Predictions of the Nonlinear Optical Properties in α-Quartz-type Germanium Oxide, J. Phys. Chem. C 116 (2012) 8692-8698.

8 A.P. Mirgorodskii, Interpretation and Calculation of Optical Vibrations in the Trigonal modification of germanium dioxide crystals, Opt. Spectrosc. 34 (1973) 667-668.

9 M. Madon, Ph. Gillet, Ch. Julien, G.D. Price, A vibrational Study of Phase Transitions Among the GeO_2 polymorphs, Phys. Chem. Miner. 18 (1991) 7-18.

10 D.V. Balitsky, V.S.Valitsky, D.Y Pushcharovsky, G.V Bondarenko, A.V Kosenko, Growth and Characterization of GeO_2 single crystals with the quartz structure, J. Crystal Growth, 180 (1997) 212-219.

11 E.R. Lippincott, A. Van Valkenburg, C.E. Weir, E.N. Bunting, Infrared studies on polymorphs of silicon dioxide and germanium dioxide, J. Res. Nat. Bureau Standards 61 (1958) 61-70.

12 R. Kaindl, D. M. Többens, S. Penner, T. Bielz, S. Soisuwan, B. Klötzer, Quantum mechanical calculations of the vibrational spectra of quartz- and rutile-type GeO_2, Phys. Chem. Minerals, 39 (2012) 47-55.

13 Kuzmenko, https://sites.google.com/site/reffitprogramm

14 E.I. Kamitsos, Y.D. Yiannopoulos, C.P. Varsamis, H. Jain, Structure-property correlation in glasses by infrared reflectance spectroscopy, J. of Non-Crystal. Solids 222 (1997) 59-68.

15 H. Djani, P. Hermet, Ph. Ghosez. First-principles characterization of the $P2_1ab$ ferroelectric phase of aurivillius Bi_2WO_6, J. Phys. Chem. C 118 (2014) 13514-13524.

16 Z.H. Levine, D.C. Allan, Linear optical response in silicon and germanium including self-energy effects, Phys. Rev. Lett. 63 (1989) 1719-1722.

17 Y. Sun, W. Xu, X. Fu, Z. Sun, J. Wang, J. Zhang, D. Rosenbach, R. Qi, K. Jiang, C. Jing, Z. Hu, X. Ma, J. Chu, J. Mater. Chem. C 5 (2017) 12792-12799.